Research Square

Preprints are preliminary reports that have not undergone peer review.
They should not be considered conclusive, used to inform clinical practice,
or referenced by the media as validated information.

A Multi-Stage EEG Hyperscanning Connectivity Framework for Robust Estimation of Inter- Brain Networks

Mahrad Ghodousi
Vilnius University
Jachin Edward Pousson
Jāzeps Vītols Latvian Academy of Music
Valdis Bernhofs
Jāzeps Vītols Latvian Academy of Music
Inga Griškova-Bulanova
inga.griskova-bulanova@gf.vu.lt

Vilnius University

Research Article

Keywords: EEG hyperscanning, inter-brain synchrony, Granger causality, phase-locking, graph metrics, biomedical signal processing, brain–computer music interface

Posted Date: September 1st, 2026

DOI: https://doi.org/10.21203/rs.3.rs-10755185/v1

License: This work is licensed under a Creative Commons Attribution 4.0 International License.
Read Full License

Additional Declarations: No competing interests reported.

Abstract

Robust estimation of inter-brain connectivity during naturalistic interaction remains a major challenge in biomedical signal processing due to shared sensory input, synchronized motor activity, and environmental confounds.

To address this problem, this study proposes and evaluates a multi-stage robust connectivity estimation pipeline for hyperscanning EEG datasets that integrates symmetric phase-based connectivity (Phase-Locking Value, PLV), directed predictive connectivity (Granger Causality, GC), and graph-theoretical network analysis. EEG was recorded simultaneously from one trained percussionist (leader) and 27 partners (followers), forming 27 leader–follower dyads/sessions, during two interaction contexts: Rehearsal (practice/learning) and Rhythmic performance (structured coordination). Connectivity estimates were subjected to surrogate-based permutation testing and recurrence-based stability filtering, followed by control-based edge exclusion using Baseline and Mechanical control conditions and ROI-level dimensionality reduction.

Connectivity related to musical interaction was predominantly expressed in the beta (13–30 Hz) and gamma (30–80 Hz) frequency bands. Rehearsal was characterized by more reciprocal directed inter-brain interactions and broader follower involvement in several network measures, whereas Rhythmic performance showed a more asymmetric topology with predominantly leader-to-follower gamma-band influence. Graph-theoretical metrics further demonstrated task-dependent reconfiguration of hyper-brain networks, with prominent condition-related effects involving frontal, centro-parietal, and parieto-occipital regions. These findings indicate that high-frequency oscillations support rapid interpersonal adaptation during joint musical performance. Methodologically, the proposed framework provides a multi-stage approach for increasing the specificity and robustness of hyperscanning connectivity estimates by reducing contributions from shared sensory, motor, and unstable connectivity patterns.

Introduction

Simultaneous recording of neural activity from interacting individuals, commonly referred to as hyperscanning, provides a framework for quantifying inter-brain coupling during real-time social behavior (Acquadro et al., 2016). From a biomedical signal processing perspective, hyperscanning poses a fundamental challenge: estimating genuine interaction-related neural connectivity in the presence of shared sensory input, synchronized motor activity, and environmental entrainment. Reliable separation of socially driven coupling from common-input artifacts therefore remains a central methodological issue in the field (Czeszumski et al., 2020).

Musical duet performance offers an ecologically structured yet experimentally controllable paradigm for investigating this problem. Joint performance requires precise sensorimotor coordination, predictive timing, error monitoring, and continuous mutual adaptation (Cheng et al., 2024; Sänger et al., 2012; Chuang et al., 2026). Because partners must dynamically align actions while maintaining role-specific contributions, musical interaction provides a natural testbed for modeling both symmetric synchrony and

directed influence between brains. Importantly, the temporal precision of musical coordination makes it particularly suitable for time-resolved connectivity analysis.

Electroencephalography (EEG) is well suited for such investigations due to its millisecond temporal resolution and tolerance to moderate movement, enabling connectivity estimation under ecologically valid interaction (Czeszumski et al., 2020; Jia et al., 2024). Prior EEG hyperscanning studies have reported inter-brain synchrony across multiple frequency bands during live musical performance (Gugnowska et al., 2022). Slower oscillations in the delta (1–4 Hz) and theta (4–8 Hz) ranges have been associated with beat alignment and shared temporal structure (Lindenberger et al., 2009; Müller et al., 2013), whereas alpha (8–12 Hz) modulation has been linked to attentional engagement (Sänger et al., 2013). Higher-frequency beta (13–30 Hz) and gamma (30–80 Hz) oscillations are frequently implicated in sensorimotor integration, predictive control, and rapid interpersonal adaptation (Astolfi et al., 2012; Zhou et al., 2016). However, the relative contribution of these frequency bands to the role-specific and task-dependent connectivity remains incompletely characterized.

Leader–follower paradigms introduce controlled asymmetry into interpersonal coordination, enabling investigation of directed information flow. Prior work suggests that leaders exhibit neural signatures consistent with proactive control, including frontal alpha suppression and midline theta activity (Konvalinka et al., 2014; Tomyta et al., 2023; Yoneta et al., 2022), whereas followers show increased engagement of temporo-parietal regions implicated in monitoring and adaptive response (Vanzella et al., 2019). Directed connectivity analyses have revealed role-dependent asymmetries in hyper-brain networks (Astolfi et al., 2011; Sänger et al., 2013). Although symmetric phase-based synchrony and directed influence have often been examined separately, recent studies have begun to integrate functional and effective connectivity measures within the same hyperscanning paradigm (Chuang et al., 2026). However, comprehensive integration of complementary connectivity measures with multi-stage robustness and confound-control procedures remains limited.

Methodologically, estimation of inter-brain connectivity during naturalistic interaction is confounded by several factors. First, common sensory input and shared motor output can artificially inflate coupling metrics if not explicitly controlled (Czeszumski et al., 2020; Li et al., 2025; Sawicki, 2025). Second, task stage (e.g., rehearsal/learning versus constrained rhythmic performance) may modulate connectivity independently of role assignment (Acquadro et al., 2016; Cheng et al., 2024). Third, high-dimensional EEG connectivity matrices are susceptible to noise amplification and instability across sessions (Chiarion et al., 2023; Tran et al., 2026). Although previous studies have implemented strategies such as metronome pacing, surrogate pairing, or time-shift controls to mitigate non-social synchrony (Bilek et al., 2015; Pan et al., 2018), comprehensive experimental control combined with analysis-level normalization remains relatively uncommon (Hu et al., 2022).

To address these limitations, the present study introduces a hyperscanning connectivity framework designed to estimate interaction-specific neural coupling under controlled naturalistic conditions. The framework integrates symmetric phase-based connectivity (Phase-Locking Value, PLV) and directed

predictive influence (Granger Causality, GC) within a unified sliding-window pipeline. Dual-layer confound control is implemented through Baseline and Mechanical control conditions, with interaction-condition edges excluded when the corresponding connections are also detected in either control condition. To enhance robustness and interpretability, edge-level stability filtering (≥ 75% recurrence across sessions) and anatomically constrained ROI aggregation are applied to reduce dimensionality and suppress spurious connections. From a biomedical signal-processing perspective, this framework functions as a multi-stage robust connectivity estimation pipeline that integrates experimental control, statistical assessment, and network-level dimensionality reduction, thereby reducing the impact of spurious edges that commonly arise in high-dimensional hyperscanning datasets.

This study therefore proposes and evaluates a multi-stage robust connectivity estimation pipeline designed for hyperscanning EEG datasets. The framework is evaluated in a musical-duet paradigm with explicitly assigned leader–follower roles and two task conditions: Rehearsal (practice/learning) and Rhythmic (structured), while keeping the musical material constant. Specifically, the study aims to: (1) quantify differences in phase synchronization (PLV) and directed predictive influence (GC) across frequency bands; (2) evaluate task-dependent network reconfiguration within the fixed-leader design; and (3) increase specificity to interaction-related connectivity by excluding connections also present in Baseline and Mechanical control conditions and by applying surrogate-based permutation testing. By combining directed and undirected connectivity measures within a controlled experimental design, this work aims to advance robust estimation of hyper-brain network topology and provide discriminative multi-band connectivity features suitable for applications in cooperative brain–computer interfaces and real-time social interaction monitoring.

Materials and Methods

Participants

Twenty-eight healthy right-handed volunteers (ages 20–40, 19 females and 9 males) participated in the study. The percussionist (a male subject) was an expert jazz drummer skilled in sight-reading and improvisation and served as the primary percussionist (further referred to as leader) in all sessions of this study. The remaining 27 participants took part in a single session and are further referred to as followers. All volunteers had normal hearing and at least five years of formal musical training. Written informed consent was obtained, and the study protocol was approved by Riga Stradiņš University Research Ethics Committee (Decision No. 2-PĒK-4/650/2023). All participants provided written consent to participate. Basic demographic and musical background information was collected prior to EEG recording.

The experimental design included a single expert leader paired with 27 followers, yielding 27 dyads and hence 27 experimental sessions (one session per follower). Leader and follower roles were explicitly assigned and implemented throughout each task; the leader identity was intentionally kept fixed across sessions to reduce task degrees of freedom and inter-session variability. Consequently, observations are

not independent with respect to leader identity, and population-level inference about “leaders” as a class is not supported. Each follower session constituted a distinct dyadic observational unit, while the leader’s EEG signal was repeatedly recorded with a different follower in each session. This fixed-leader configuration was selected to maximize experimental control over performance timing and role implementation while enabling evaluation of the proposed connectivity framework across multiple dyads.

Experimental Design and Procedure

Each experimental session, lasting about 3 hours, involved one follower and the leader in a specialized lab designed to minimize noise. Each session followed a fixed sequence of task conditions, with Rehearsal serving as a practice/learning phase before the subsequent Rhythmic performance trials, with brief breaks between conditions. The protocol included a 20-second Baseline condition as well as Mechanical, Rehearsal, and Rhythmic conditions (Fig. 1; full details are provided in Table S1 in the Supplementary Material). The musical tasks were initially designed to observe the shift from synchronized rhythmic playing to spontaneous improvisation, capturing IBS (Inter- and Intra-brain Synchronizations) and information flows in both coordination- and creativity-oriented tasks. The current analysis focused only on the coordination-oriented conditions: Baseline, Mechanical, Rhythmic, and Rehearsal.

EEG Acquisition

EEG data from the leader and follower were recorded simultaneously using two identical 32-channel EEG systems (Enobio 32, Neuroelectrics, Spain; Fig. 2, bottom-left panel), with Ag/AgCl electrodes placed according to the international 10–20 system and CMS/DRL electrodes on the right earlobe for reference and grounding. Signal quality (line noise, main noise, offset, drift) was monitored via Neuroelectrics Instrument Controller v.2.0.11.1, and EEG hyperscanning data was synchronized sample to sample at 500 Hz using the Lab Streaming Layer (LSL) protocol on a central computer. Custom software controlled trial sequencing, marked task onsets/offsets (Baseline, Mechanical, Rehearsal), displayed a 3 s countdown, and presented the 32-beat Rhythmic score to the percussionist. For Rehearsal and Rhythmic runs, participants used MIDI percussion pads (Roland SPD-30 Octopad); MIDI onsets were sent as LSL markers to both EEG streams and recorded by a second computer. This setup ensured sub-millisecond alignment of EEG, task, and performance events.

EEG Preprocessing

All EEG data were processed using EEGLAB (MATLAB) (Delorme & Makeig, 2004) and custom scripts. The recordings were synchronized using the initial trigger to ensure both datasets started simultaneously, and the data were then trimmed to equal lengths. For artifact removal, the leader and follower EEG channels were concatenated into a single 64-channel dataset. EEGLAB’s clean_rawdata

function was used to remove channels or data segments exhibiting abnormal amplitudes or excessive noise. Datasets retaining less than 80% of the original signal duration or containing more than two removed channels after cleaning were excluded from further analysis. No dataset met these exclusion criteria. Thus, all datasets were retained, and removed channels (< 3 per dataset) were interpolated. A band-pass filter (zero-phase, linear finite impulse response (FIR) filter implemented in EEGLAB using pop_eegfiltnew), with cutoff frequencies of 0.5–80 Hz, and a 50 Hz notch filter were applied to suppress interference. The filtered data were then separated back into leader and follower channel sets, and Independent Component Analysis (ICA) was performed on each 32-channel dataset. Components associated with eye blinks, eye movements, muscle activity, or cardiac artifacts were removed. Finally, the data from each subject were re-referenced to the average of the T7 and T8 (temporal) channels to minimize common noise while preserving comparability with our prior connectivity work (Ghodousi et al., 2022, 2023), leaving 30 analysis channels per participant (60 channels per dyad). Using event markers, each continuous EEG recording was segmented into discrete epochs corresponding to individual trials and conditions.

Connectivity Estimation Framework

Inter-brain and intra-brain connectivity were estimated using complementary undirected (Phase-Locking Value, PLV) and directed (Granger Causality, GC) measures within a unified time-resolved framework. The overall processing pipeline of the proposed hyperscanning connectivity framework is illustrated in Fig. 2. All analyses were performed separately for the delta (0.5–4 Hz), theta (4–8 Hz), alpha (8–12 Hz), beta (13–30 Hz), and gamma (30–80 Hz) frequency bands. To capture non-stationary interaction dynamics, connectivity was computed using a sliding-window approach with 3 s window length and 1 s step size. Window length was selected to ensure sufficient frequency resolution in the beta and gamma bands while maintaining temporal sensitivity to interaction-related changes.

Hyperscanning Connectivity Pipeline

The proposed hyperscanning analysis framework consists of sequential processing stages designed to improve the robustness and specificity of interaction-related connectivity estimates. First, preprocessing and artifact suppression were applied to remove non-neural signal components. Second, time-resolved connectivity was estimated using complementary directed (Granger Causality, GC) and phase-based (Phase-Locking Value, PLV) metrics within sliding windows. Third, surrogate-based permutation testing was applied separately to GC and PLV connections to determine the significance of individual intra- and inter-brain edges relative to surrogate data. Fourth, recurrence-based stability filtering retained only connections consistently observed across sessions and trials, thereby reducing spurious edges arising from noise or transient fluctuations. Fifth, control-based edge exclusion was applied to the Rehearsal and Rhythmic matrices by removing recurrent significant edges that were also detected in either the Baseline or Mechanical control condition. Finally, channel-level connectivity matrices were aggregated at

the ROI level to reduce dimensionality and facilitate graph-theoretical characterization of hyper-brain network topology.

Analysis

Granger Causality

Granger causality (GC) is a statistical measure of directed predictive influence between time series. A signal $Y$is said to Granger-cause a signal X if past values of Y improve the prediction of future values of X beyond what can be achieved using only the past of X itself (Ghodousi et al., 2022; Tafreshi et al., 2019).

For two time series $x\left(t\right)$ and $y\left(t\right)$, Granger causality was evaluated using an autoregressive modeling framework. First, a restricted autoregressive (AR) model of order $p$was fitted to $x\left(t\right)$ (1):

$$x_t = c + \sum_{k=1}^{p} \phi_k x_{t-k} + \epsilon_t \qquad (1)$$

where ϵ_t is the residual prediction error. The residual variance of this model is denoted σ_R^2.

Next, an unrestricted model including past values of both x and y was estimated (2):

$$x_t = c + \sum_{k=1}^{p} \phi_k x_{t-k} + \sum_{k=1}^{q} \theta_k y_{t-k} + u_t \qquad (2)$$

where $u_t$represents the new residual error with variance σ_U^2.

The optimal lag orders p and q were selected using the Bayesian Information Criterion (BIC) within each analysis window, constrained by a predefined maximum lag. Model selection was performed separately for the restricted and unrestricted formulations.

Granger causality from y to x was then assessed using an F-test comparing the residual sums of squares of the restricted (RSS_R) and unrestricted (RSS_U) models (3):

$$F = \frac{(RSS_R - RSS_U)/q}{RSS_U/(T-(p+q+1))} \qquad (3)$$

where T is the number of observations in the window and q is the number of additional parameters introduced by including past values of y. Directed connectivity was estimated using pairwise autoregressive Granger causality in sliding 3-s windows (1500 samples at 500 Hz), with model order selected automatically up to a maximum lag of 500 ms ($p \leq 250$). The GC implementation internally used an F-test to assess whether inclusion of the source-signal history improved prediction of the target signal relative to the restricted model. The resulting GC estimates were subsequently subjected to the surrogate-based permutation testing described below, which provided the edge-level significance criterion used for subsequent processing.

Phase-Locking Value

Phase-locking value (PLV) captures the synchronization or phase stability between oscillatory signals (Lachaux et al., 1999). For each pair of EEG signals X and Y, PLV is defined as (4):

$$PLV_{XY} = abs\left(\frac{1}{T}\sum_{t=1}^{T} e^{i(\Phi_X(t)-\Phi_Y(t))}\right)$$

4

where $\Phi_X(t)$ and $\Phi_Y(t)$ denote the instantaneous phases of signals X and Y at time t, respectively, and $T$is the number of time points in the analyzed segment. The instantaneous phase $\Phi_X(t)$ was obtained from the analytic signal computed via the Hilbert transform (5),

$$z_X(t) = X(t) + i\hspace{0.17em}\mathcal{H}\{X(t)\} = A_X(t)\, e^{i\Phi_X(t)}$$

5

where $\mathcal{H}\{\cdot\}$ denotes the Hilbert transform, $A_X(t)$ is the instantaneous amplitude, and $\Phi_X(t) = arg(z_X(t))$(analogously for $\Phi_Y(t)$).

PLV values range from 0 to 1, with values close to 1 indicating a stable phase difference between X and Yacross time (strong phase synchronization), and values close to 0 indicating a random or inconsistent phase relationship.

Connectivity calculation framework

For each frequency band, GC and PLV were used to reveal asymmetric (directional) and symmetric (undirected) connectivity between every pair of EEG channels from the leader and follower. Measures were computed using a sliding-window approach applied to temporally corresponding trials from the leader and follower, allowing estimation of both intra-brain and inter-brain connectivity within a single connectivity matrix. Connectivity matrices obtained from all sliding windows within each paired trial were averaged, yielding a single 60 × 60 connectivity matrix per leader–follower trial pair and condition (30 channels from the leader and 30 from the follower).

Statistical Validation of connections

Statistical significance was assessed separately for GC and PLV using surrogate-based permutation testing applied to every channel-pair connection within individual trials, including both intra-brain and inter-brain edges. For each measure, a null distribution was generated by circularly shifting one time series relative to the other (1,000 permutations) while preserving the same testing framework across Baseline, Mechanical, Rhythmic, and Rehearsal conditions. Connections were considered significant when the observed connectivity exceeded the 99th percentile of the corresponding surrogate distribution

($p < 0.01$). Non-significant connections were set to zero, and only significant connections were retained for subsequent processing.

Edge-Level Stability Filtering

To enhance robustness and suppress session-specific artifacts, GC and PLV connections were retained only if present (i.e., significant and non-zero) in ≥ 75% of the relevant matrices across all sessions and trials. The same recurrence criterion was applied separately to each connectivity measure. A 75% recurrence threshold was selected as a conservative stability criterion to retain edges showing substantial cross-session consistency while avoiding excessive sparsification of interaction-related networks. This recurrence-based filter was used as a stability constraint rather than as an additional inferential significance test.

Interaction-Specific Control-Based Edge Exclusion

To increase specificity to interpersonal interaction, connectivity estimation, surrogate-based significance testing, and recurrence-based stability filtering were first applied separately to the Baseline, Mechanical, Rhythmic, and Rehearsal conditions. Rehearsal and Rhythmic matrices were then subjected to control-based edge exclusion: a recurrent significant edge in an interaction condition was set to zero if the corresponding edge was also present in either the Mechanical or Baseline matrix. Thus, the retained Rehearsal and Rhythmic networks contained recurrent significant connections that were not detected in the control conditions, reducing contributions associated with baseline coupling and repeated motor activity.

ROI-Level Dimensionality Reduction

To reduce dimensionality and improve interpretability, electrodes were grouped into 10 anatomically defined regions of interest (ROIs) per brain (Ghodousi et al., 2022): mid-frontal left (1) and right (2), left (3) and right (4) frontal, centro-parietal left (5) and right (6), parieto-occipital left (7) and right (8), fronto-central (9) and central parieto-occipital (10). Channel-level connectivity values were averaged across ROI pairs, yielding a 20 × 20 connectivity matrix representing mesoscopic network topology. This spatial aggregation reduces variance, mitigates multiple-comparison burden, and enhances anatomical interpretability.

Statistical Validation and Network Characterization

Standard graph-theoretic network measures were computed separately from ROI-level GC and PLV networks using the Brain Connectivity Toolbox (Rubinov & Sporns, 2010), including degree (ND), strength (NS), and betweenness (NB) centrality for each trial. For directed GC networks, ND was defined as out-degree (the number of outgoing connections) and NS as out-strength (the sum of the weights of outgoing connections); for undirected PLV networks, degree and strength reflected the number and summed weights of incident connections, respectively. Metrics were calculated separately for intra-brain and inter-brain networks. To assess differences between Rehearsal and Rhythmic conditions, Wilcoxon rank-sum tests were used as an exploratory comparison of trial-level graph-metric distributions pooled

across the 27 sessions. Because the fixed leader contributed repeatedly across sessions and trial-level observations are nested within dyads, these tests are interpreted as exploratory rather than as independent-participant population inference. Effect sizes were quantified using the absolute value of Cohen's *d* (|*d*|) to characterize the magnitude of condition differences, irrespective of direction. Given the exploratory ROI-level analysis and the use of several graph metrics, frequency bands, and connectivity categories, no additional family-wise multiple-comparison correction was imposed; results were instead interpreted together with effect sizes, recurrence filtering, and leave-one-follower-out (LOFO) robustness assessment.

To assess robustness to any single follower/dyad, the complete statistical comparison was repeated 27 times using a LOFO procedure, with one follower session omitted in each iteration. For every ROI/metric cell, each iteration produced a p-value/significance level and a Cohen's d. A cell was retained as robust only when it remained statistically significant in all 27 LOFO iterations. For retained cells, Figs. 5 and 6 report the least significant (i.e., most conservative) significance category observed across the 27 runs, while the displayed effect size is the arithmetic mean of the absolute Cohen's d across the 27 LOFO iterations. This procedure was used as a robustness assessment of the exploratory condition comparisons rather than as an independent validation dataset.

To summarize the spatial convergence of condition-related effects across connectivity measures, an integrated ROI-level representation was constructed from the GC- and PLV-derived graph-metric results. For each ROI and connectivity category (GC intra-brain, GC inter-brain, PLV intra-brain, and PLV inter-brain), the graph metric showing the strongest statistical evidence among Node Betweenness, Node Strength, and Node Degree was selected. Statistical evidence was based on the conservative LOFO result, with only effects that remained significant across all 27 leave-one-follower-out iterations considered. For each selected ROI-level effect, the corresponding mean |Cohen's d| acrossLOFO iterations was retained for visualization. This procedure was intended as a descriptive integration of the ROI-level findings rather than as an additional inferential analysis.

Results

Connectivity results were analyzed at three complementary levels. Directed connectivity (GC) quantified directional information flow, whereas phase-based connectivity (PLV) assessed symmetric synchronization between signals. Graph-theoretical metrics derived from these connectivity matrices were then used to characterize task-dependent network organization.

Application of the proposed hyperscanning connectivity framework revealed stable task-dependent patterns of inter-brain connectivity. After surrogate-based permutation validation, recurrence-based stability filtering, and control-based edge exclusion, approximately 46.3 ± 3% (mean ± SD) of candidate connections remained, with surviving edges concentrated within the beta (13–30 Hz) and gamma (30–80 Hz) frequency bands, whereas lower-frequency bands showed only sparse surviving connections. This reduction indicates that the proposed pipeline effectively suppressed unstable or non-specific

edges while preserving consistent interaction-related connectivity patterns. Across both connectivity measures, hyper-brain network organization differed between the Rehearsal and Rhythmic conditions. Differences between the Rhythmic condition and the Rehearsal condition were reflected in the density, directionality, and spatial distribution of surviving connections. However, as shown in the graph-theoretical analysis, GC and PLV differed in the network components in which these effects were most pronounced. The following sections describe these results in detail, first examining GC, then PLV, and finally network-level differences revealed by graph-theoretical metrics.

Granger Causality

Directed connectivity analysis revealed that interaction-related GC was primarily concentrated in the beta (13–30 Hz) and gamma (30–80 Hz) frequency bands after surrogate-based permutation validation and recurrence filtering. All reported GC networks represent interaction-specific connectivity after exclusion of edges also detected in the Baseline or Mechanical control conditions. Figure 3 illustrates the control-filteredintra- and inter-brain GC networks for both task conditions.

Intra-brain GC

Intra-brain directed connectivity was concentrated in the beta and gamma bands and showed stronger task-dependent modulation in the follower network than in the leader network. In the follower, gamma-band connectivity during the Rhythmic condition was centered in right frontal and parieto-occipital regions, whereas the Rehearsal condition engaged broader frontal areas, including bilateral mid-frontal and frontal-lateral regions with additional beta-band recruitment of left parieto-occipital. In contrast, the leader network exhibited comparatively stable connectivity across conditions, with limited beta-band involvement in the centro-parietal areas. Also in the gamma band, both conditions involved the left parieto-occipital regions. However, the Rhythmic condition showed broader involvement of the right centro-parietal regions, whereas the Rehearsal condition was characterized by broader involvement of the left fronto-lateral region.

Inter-brain GC

Inter-brain GC revealed clear task-dependent differences in the directionality of information flow between the leader and follower networks. During the Rhythmic condition, gamma-band connectivity exhibited a predominantly asymmetric topology, with directed influences originating mainly from the leader's centro-parietal and parieto-occipital, and frontal regions toward frontal and parieto-occipital areas of the follower. In contrast, the Rehearsal condition showed a denser and more reciprocal pattern of directed interactions, with additional follower-to-leader influences emerging from frontal and parieto-occipital regions, resulting in a more bidirectional network organization.

Phase-Locking Value

Phase-based synchronization analysis revealed condition-dependent modulation of connectivity in the beta and gamma bands, with distinct spatial patterns emerging across leader and follower networks.

Figure 4 presents the control-filtered group-averaged PLV connectivity matrices for both task conditions and frequency bands.

Intra-brain PLV

Intra-brain synchronization showed distinct spatial patterns across task conditions. During the Rhythmic condition, the follower exhibited widespread gamma-band synchronization across frontal, centro-parietal, and parieto-occipital regions, whereas beta-band synchronization was mainly confined to centro-parietal and parieto-occipital regions. In contrast, the leader showed comparatively more localized gamma-band synchronization, predominantly within frontal regions, while beta-band synchronization was more widespread. During the Rehearsal condition, the follower demonstrated widespread beta-band synchronization, particularly in the centro-parietal region, whereas gamma-band synchronization was comparatively limited to frontal regions. The leader network continued to exhibit relatively localized and weaker gamma-band synchronization, mainly in the centro-parietal and parieto-occipital regions, while beta-band synchronization was more widespread but remained weaker than that observed in the follower.

Inter-brain PLV

Inter-brain PLV demonstrated a clear task-dependent redistribution of symmetric coupling between the two networks. During the Rhythmic condition, synchronization between the two brains was relatively sparse and was dominated by beta-band coupling, primarily involving centro-parietal and parieto-occipital regions. In contrast, the Rehearsal condition exhibited markedly stronger gamma-band synchronization centered on centro-parietal, parieto-occipital, and fronto-central regions, while beta-band coupling showed a redistribution of synchronized regions rather than a simple increase in spatial extent. These results indicate that the Rehearsal condition was associated with increased gamma-band phase synchronization across the two brains relative to the subsequent Rhythmic performance condition.

Statistical Comparison of Network Metrics

To quantify task-dependent changes in hyper-brain network organization, graph-theoretical metrics including node degree (ND), node strength (NS), and betweenness centrality (NB) were compared between the Rehearsal and Rhythmic conditions in the beta and gamma frequency bands for both GC- and PLV-derived networks. Statistical comparisons used exploratory Wilcoxon rank-sum tests on trial-level graph-metric distributions, followed by a 27-iteration LOFO robustness assessment. A result was displayed as significant only when the corresponding cell remained significant in all 27 LOFO iterations; the asterisk level represents the least significant category observed across those iterations. Effect sizes are reported as the mean Cohen’s d across the 27 LOFO iterations. Figures 5 and 6 summarize these conservative significance levels and mean effect sizes for GC- and PLV-derived networks.

GC-derived networks

Graph metrics derived from GC networks showed the strongest condition-dependent effects within the follower network, indicating that directed connectivity patterns were particularly sensitive to task structure. Differences between the Rehearsal and Rhythmic conditions were most consistently reflected in node degree and node strength, suggesting that task context primarily modulated the number and cumulative weight of directed connections rather than the global routing role of nodes. These effects were most prominent in the gamma band, where several follower ROIs exhibited higher ND and NS. In contrast, the leader network showed comparatively fewer significant GC-based changes across conditions, particularly within the intra-brain networks. (Fig. 5).

PLV-derived networks

In contrast to the GC results, graph metrics derived from the PLV networks showed more pronounced condition-related modulation within the leader network, particularly in the intra-brain synchrony. Node Strength and Node Degree again emerged as the most discriminative graph metrics for inter-brain synchronization. In contrast, within the intra-brain networks, Node Betweenness also emerged as a sensitive metric for distinguishing between the two task conditions, whereas Node Degree exhibited comparatively fewer significant changes. Unlike the GC results, both the leader and follower networks exhibited significant condition-related modulation in the PLV analysis. Furthermore, although significant effects were observed in both frequency bands, a greater number of highly significant regions were identified in the gamma band than in the beta band (Fig. 6).

Dissociation between directed and phase-based network effects

Taken together, these results reveal a metric- and role-dependent dissociation in network reconfiguration. Directed connectivity metrics (GC) were more sensitive to task-dependent changes in the follower network, particularly in the gamma band, whereas symmetric phase-based metrics (PLV) showed stronger modulation in the leader network, especially in the intra-brain networks and across both beta and gamma frequency bands. This complementary pattern indicates that directed information flow and phase synchronization capture distinct aspects of dyadic coordination: GC is more sensitive to changes in directional communication associated with the follower's adaptive role, whereas PLV emphasizes task-dependent modulation of oscillatory synchronization specially within the leader's functional network.

Robustness of effects

Across both GC and PLV analyses, the cells displayed as significant in Figs. 5 and 6 remained significant in all 27 LOFO iterations. For each retained cell, the asterisks in the Figures correspond to the least significant category observed across the iterations, and effect-size shading represents the mean Cohen’s d across the 27 runs. This conservative summary indicates that the reported condition differences were not dependent on omission of any single follower session.

Summary of Convergent Regional Effects

To identify spatial convergence across analyses, ROIs involved in both directed (GC) and phase-based (PLV) connectivity were summarized in Fig. 7 by integrating the ROI-level statistical results from Figs. 5 and 6. For each brain region and connectivity category (GC intra-brain, GC inter-brain, PLV intra-brain, and PLV inter-brain), the graph metric with the strongest statistical evidence among Node Betweenness, Node Strength, and Node Degree was selected. Figure 7 displays these selected ROI-level results across the full effect-size scale used in the heatmap. As a more stringent illustrative summary, considering regions with $p < 0.05$ and mean |Cohen's d| > 0.75, the leader showed prominent effects in the centro-parietal right, parieto-occipital left, and central parieto-occipital regions, whereas the follower showed a broader pattern involving the fronto-lateral left, parieto-occipital left and right, fronto-central, and central parieto-occipital regions. Notably, effects in the parieto-occipital left and central parieto-occipital regions were observed in both the leader and follower networks, suggesting that these regions may represent common sites of task-related cortical engagement. In contrast, the additional involvement of fronto-lateral and fronto-central regions in the follower suggests a more spatially distributed pattern of cortical recruitment.

Discussion

This study investigated frequency-, role-, and task-dependent patterns of inter-brain connectivity during musical interaction using a dual-EEG hyperscanning analysis pipeline combining directed (GC) and phase-based (PLV) measures. The proposed multi-stage framework was designed to improve the robustness and interpretability of hyperscanning connectivity estimates while suppressing spurious coupling arising from shared input and high-dimensional noise. This approach enabled complementary assessment of phase synchronization (PLV) and directed predictive information flow (GC), in line with recommendations emphasizing the importance of distinguishing undirected synchrony from directional predictive influence in social interaction analyses (Czeszumski et al., 2020; Dumas et al., 2010; Konvalinka & Roepstorff, 2012; Friston, 2011). Three main findings emerged. First, interaction-related connectivity was concentrated in the beta and gamma frequency bands. Second, task structure strongly shaped hyper-brain network topology: the Rhythmic performance condition showed predominantly leader-driven connectivity, whereas the Rehearsal condition was characterized by broader and more reciprocal interactions. Third, convergent patterns across GC and PLV analyses identified common sites of task-related network engagement in frontal, centro-parietal, and parieto-occipital regions. Within the present fixed-leader configuration, these patterns reflect reproducible task- and role-dependent interaction effects across follower sessions rather than population-level generalization to leaders as a class.

Connectivity was primarily concentrated in the beta (≈ 13–30 Hz) and gamma (≈ 30–80 Hz) bands, frequencies often linked to sensorimotor coordination and predictive timing. Connectivity patterns differed between task conditions: Rehearsal was characterized by more reciprocal directed inter-brain connectivity and broader follower involvement in several network measures, whereas Rhythmic

performance exhibited predominantly leader-to-follower directed influence, consistent with previous evidence that leader–follower interactions can exhibit role-dependent asymmetries in effective inter-brain connectivity (Sänger et al., 2013; Chuang et al., 2026). Because edges also present in the Baseline or Mechanical control conditions were excluded, the retained networks are less likely to be dominated by baseline coupling or repeated motor activity. The surviving connectivity is therefore interpreted as being more specific to interpersonal musical coordination, while residual shared-input effects cannot be completely excluded. This interpretation is consistent with prior work showing that inter-brain synchrony diminishes in non-interactive or pseudo-pair conditions (Chabin et al., 2022), highlighting the importance of controlling for shared sensory entrainment and motor execution that can otherwise inflate coupling estimates (Czeszumski et al., 2020; Leahy et al., 2025).

Beyond confirming the stability of the reported connectivity patterns, the present results also demonstrate the methodological advantages of the proposed multi-stage connectivity estimation framework. The combination of surrogate-based permutation testing, recurrence-based stability filtering, control-based edge exclusion, and ROI-level dimensionality reduction reduces the influence of spurious connections that commonly arise in high-dimensional connectivity analyses and hyperscanning datasets (Bastos & Schoffelen, 2016; Friston, 2011). In addition, integrating directed (GC) and undirected (PLV) connectivity measures provides complementary sensitivity to both directed predictive influence and phase synchronization (Bastos & Schoffelen, 2016; Seth et al., 2015; Chuang et al., 2026). The consistency of the observed patterns across the 27 LOFO iterations supports the robustness of the reported condition-related effects within the present dataset, indicating that these effects were not driven by any single follower/dyad. As with most EEG-based connectivity analyses, residual effects of volume conduction and shared reference cannot be fully excluded, although the combination of surrogate-based testing and recurrence filtering reduces the likelihood that such artifacts drive the reported network patterns. More broadly, the framework provides a modular analysis architecture that can be adapted to other naturalistic hyperscanning settings in which reliable connectivity estimation requires simultaneous control of statistical validity, cross-session stability, and anatomical interpretability.

Importantly, convergent regional patterns emerged across the directed (GC) and phase-based (PLV) analyses. Across these complementary measures, condition-related effects repeatedly involved parieto-occipital and frontal regions in the follower network and centro-parietal and parieto-occipital regions in the leader network. This cross-metric convergence suggests that these regions represent common sites of task-related network engagement rather than effects restricted to a single connectivity measure. The prominence of parietal and parieto-occipital regions is consistent with their established roles in visuomotor integration, external monitoring, and action coordination during joint performance (Sänger et al., 2012; Zhou et al., 2016).

Frequency-specific analyses further showed that intra- and inter-brain coupling was concentrated in beta and gamma bands, with minimal surviving connectivity in delta, theta, or alpha ranges. Gamma-band connectivity was particularly pronounced and spatially distributed during Rehearsal, which may reflect

the greater demands for rapid adjustment and interpersonal adaptation during the practice/learning phase. The control-based exclusion of GC and PLV edges also detected in the Baseline or Mechanical conditions may have increased the specificity of the retained networks to faster oscillatory processes involved in real-time adaptation, error monitoring, and fine-grained sensorimotor coordination (Astolfi et al., 2012; Konvalinka et al., 2014; Yoneta et al., 2022; Zhou et al., 2016). However, the comparatively sparse delta-band connectivity should be interpreted cautiously because estimation at the lowest frequencies was constrained by the 3-s analysis window.

Methodologically, the inclusion of Baseline and Mechanical control conditions at both the experimental and analytical levels enabled control-based exclusion of connectivity patterns also present in these control conditions.. This procedure reduced connectivity patterns attributable to baseline coupling and repeated motor processes, thereby increasing the specificity of the retained networks to interpersonal musical coordination. The control-based approach complements surrogate-pair and time-shift approaches (Bilek et al., 2015; Pan et al., 2018) and provides an ecologically grounded strategy for reducing non-interaction-related contributions in live performance contexts.

Taken together, the findings highlight three principles of inter-brain coordination in joint music-making. First, hyper-brain topology differed between the Rehearsal and Rhythmic conditions, with Rehearsal showing broader and more reciprocal connectivity. Second, within the explicitly assigned fixed leader–follower configuration, the two task stages were associated with different patterns of directed predictive information flow, with Rhythmic performance showing greater leader-to-follower influence and Rehearsal showing greater reciprocity. The latter may reflect the greater demands for ongoing adjustment during the practice/learning phase. Third, beta- and gamma-band oscillations emerge as key frequency channels for dyadic coordination, offering discriminative features for connectivity modeling and potential applications in Brain–Computer Music Interface (BCMI) systems. Multi-band feature extraction therefore appears essential for applied hyperscanning research, with higher-frequency coupling supporting rapid dyadic adaptation and slower oscillations potentially indexing broader engagement dynamics (Rai et al., 2025).

Beyond the specific musical interaction paradigm used for evaluation, the present study introduces a methodological framework for robust estimation of inter-brain connectivity in hyperscanning datasets. The integration of complementary connectivity metrics (GC and PLV), surrogate-based permutation testing, recurrence-based stability filtering, control-based edge exclusion, and ROI-level dimensionality reduction provides a multi-stage strategy for suppressing spurious coupling arising from common input and high-dimensional noise. These methodological components may be applicable to a wide range of hyperscanning contexts including cooperative brain–computer interfaces, multi-user neurotechnology, and studies of naturalistic social interaction.

Limitations and future directions

While the present study demonstrates robust task- and role-dependent connectivity patterns within a controlled hyperscanning paradigm, several design constraints limit the scope of inference. First, the study employed a single expert leader paired with multiple followers, meaning that leader-related connectivity patterns may partly reflect individual characteristics rather than general properties of leadership. Future studies should include multiple leaders and counterbalanced role assignments to separate role effects from individual traits. Second, Rehearsal served as a practice/learning phase and preceded Rhythmic performance within the fixed experimental sequence. Consequently, differences between these conditions may reflect not only task-related network reconfiguration but also practice, familiarization, or order effects. Future studies using counterbalanced or independently matched conditions are needed to separate these contributions. Third, despite surrogate-based permutation testing, control-based edge exclusion, and ≥ 75% cross-session recurrence filtering, the sample size (27 dyads) limits statistical power for detecting subtle network effects. The ROI-level condition comparisons were exploratory and no formal family-wise multiple-comparison correction was applied; therefore, individual p-values should be interpreted together with effect sizes, recurrence stability, and the LOFO robustness analysis rather than as confirmatory tests. Larger cohorts would allow more precise modeling of inter-individual variability. Fourth, pairwise Granger causality does not fully account for multivariate dependencies or common drivers across channels. Future work could therefore apply multivariate or ROI-level connectivity models. Finally, the EEG spatial resolution and structured percussion paradigm limit anatomical specificity and generalization to other interaction types. Multimodal imaging and more diverse interaction contexts would help extend the present framework.

Conclusions

This study introduced and evaluated a robust EEG hyperscanning connectivity framework for estimating interaction-related neural coupling during naturalistic social interaction. Leader and follower roles were explicitly assigned throughout the experiment, while the same expert leader was intentionally retained across all 27 dyads to reduce task degrees of freedom and inter-session variability. Within this fixed-leader design, the Rehearsal and Rhythmic task stages were associated with systematic differences in hyper-brain network topology. Connectivity was primarily expressed in the beta and gamma bands, with the Rehearsal practice/learning phase showing more reciprocal coupling and subsequent Rhythmic performance showing greater leader-to-follower directed predictive influence. Control-based edge exclusion was used to increase the specificity of the retained connectivity patterns by excluding edges also present during Baseline or Mechanical conditions. The integration of phase-based and directed predictive connectivity measures within a multi-stage estimation pipeline provides a robust framework for characterizing neural coupling in social interaction. Beyond advancing the neuroscience of joint action, these findings highlight the potential of hyperscanning-derived features for connectivity modeling, cooperative BCI development, and Brain–Computer Music Interface applications.

Declarations

Ethics declaration

The study was approved by Riga Stradiņš University Research Ethics Committee (Decision No. 2-PĒK-4/650/2023). All participants provided written consent to participate.

Funding declaration

No funding was recieved for this research.

Author Contribution

Conceptualization, I.G.-B., J.E.P. and V.B.; methodology, M.G., J.E.P. and I.G.-B.; software, M.G.; formal analysis, M.G. and I.G.-B.; investigation, J.E.P.; resources, V.B.; writing—original draft preparation, I.G.-B., M.G.; writing—review and editing, I.G.-B., M.G., J.E.P., V.B. All authors have read and agreed to the published version of the manuscript.

Data Availability

The datasets generated and/or analysed during the current study are available from the corresponding author on reasonable request, subject to applicable ethical approvals and data protection regulations.

Data availability

The datasets generated and/or analysed during the current study are available from the corresponding author on reasonable request, subject to applicable ethical approvals and data protection regulations.

Competing Interest declaration

The authors declare no competing interests.

Author Contribution declaration

Conceptualization, I.G.-B., J.E.P. and V.B.; methodology, M.G., J.E.P. and I.G.-B.; software, M.G.; formal analysis, M.G. and I.G.-B.; investigation, J.E.P.; resources, V.B.; writing—original draft preparation, I.G.-B., M.G.; writing—review and editing, I.G.-B., M.G., J.E.P., V.B. All authors have read and agreed to the published version of the manuscript.

Clinical trial number

Clinical trial number
Not applicable.

References

1. Acquadro MAS, Congedo M, De Riddeer D (2016) Music Performance As an Experimental Approach to Hyperscanning Studies. *Frontiers in Human Neuroscience*, *10*. https://doi.org/10.3389/fnhum.2016.00242
2. Astolfi L, Toppi J, Borghini G, Vecchiato G, He EJ, Roy A, Cincotti F, Salinari S, Mattia D, He B, Babiloni F (2012) Cortical activity and functional hyperconnectivity by simultaneous EEG recordings from interacting couples of professional pilots. *2012 Annual International Conference of the IEEE Engineering in Medicine and Biology Society*, 4752–4755. https://doi.org/10.1109/EMBC.2012.6347029
3. Astolfi L, Toppi J, Borghini G, Vecchiato G, Isabella R, De Vico Fallani F, Cincotti F, Salinari S, Mattia D, He B, Caltagirone C, Babiloni F (2011) Study of the functional hyperconnectivity between couples of pilots during flight simulation: An EEG hyperscanning study. *2011 Annual International Conference of the IEEE Engineering in Medicine and Biology Society*, 2338–2341. https://doi.org/10.1109/IEMBS.2011.6090654
4. Bastos AM, Schoffelen J-M (2016) A Tutorial Review of Functional Connectivity Analysis Methods and Their Interpretational Pitfalls. *Frontiers in Systems Neuroscience*, *9*. https://doi.org/10.3389/fnsys.2015.00175
5. Bilek E, Ruf M, Schäfer A, Akdeniz C, Calhoun VD, Schmahl C, Demanuele C, Tost H, Kirsch P, Meyer-Lindenberg A (2015) Information flow between interacting human brains: Identification, validation, and relationship to social expertise. *Proceedings of the National Academy of Sciences*, *112*(16), 5207–5212. https://doi.org/10.1073/pnas.1421831112
6. Bullmore E, Sporns O (2009) Complex brain networks: graph theoretical analysis of structural and functional systems. Nat Rev Neurosci 10(3):186–198. https://doi.org/10.1038/nrn2575
7. Chabin T, Gabriel D, Comte A, Pazart L (2022) Audience Interbrain Synchrony During Live Music Is Shaped by Both the Number of People Sharing Pleasure and the Strength of This Pleasure. *Frontiers in Human Neuroscience*, *16*. https://doi.org/10.3389/fnhum.2022.855778
8. Cheng S, Wang J, Luo R, Hao N (2024) Brain to brain musical interaction: A systematic review of neural synchrony in musical activities. Neurosci Biobehavioral Reviews 164:105812. https://doi.org/10.1016/j.neubiorev.2024.105812
9. Chiarion G, Sparacino L, Antonacci Y, Faes L, Mesin L (2023) Connectivity analysis in EEG data: A tutorial review of the state of the art and emerging trends. Bioengineering 10(3):372. https://doi.org/10.3390/bioengineering10030372
10. Chuang C-H, Peng P-H (2026) Neural synchrony and cognitive map formulation in collaborative navigation: Leader-follower couplings revealed by EEG hyperscanning. Cogn Neurodyn 20:149. https://doi.org/10.1007/s11571-026-10521-4
11. Czeszumski A, Eustergerling S, Lang A, Menrath D, Gerstenberger M, Schuberth S, Schreiber F, Rendon ZZ, König P (2020) Hyperscanning: A Valid Method to Study Neural Inter-brain

Underpinnings of Social Interaction. *Frontiers in Human Neuroscience*, *14*. https://doi.org/10.3389/fnhum.2020.00039

12. Delorme A, Makeig S (2004) EEGLAB: an open source toolbox for analysis of single-trial EEG dynamics including independent component analysis. J Neurosci Methods 134(1):9–21. https://doi.org/10.1016/j.jneumeth.2003.10.009
13. Dumas G, Lachat F, Martinerie J, Nadel J, George N (2010) Inter-brain synchronization during social interaction. PLoS ONE, 5(8), e12166
14. Friston KJ (2011) Functional and Effective Connectivity: A Review. Brain Connect 1(1):13–36. https://doi.org/10.1089/brain.2011.0008
15. Ghodousi M, Pousson JE, Bernhofs V, Griškova-Bulanova I (2023) Assessment of Different Feature Extraction Methods for Discriminating Expressed Emotions during Music Performance towards BCMI Application. Sensors 23(4):2252. https://doi.org/10.3390/s23042252
16. Ghodousi M, Pousson JE, Voicikas A, Bernhofs V, Pipinis E, Tarailis P, Burmistrova L, Lin Y-P, Griškova-Bulanova I (2022) EEG Connectivity during Active Emotional Musical Performance. Sensors 22(11):4064. https://doi.org/10.3390/s22114064
17. Gugnowska K, Novembre G, Kohler N, Villringer A, Keller PE, Sammler D (2022) Endogenous sources of interbrain synchrony in duetting pianists. Cereb Cortex 32(18):4110–4127. https://doi.org/10.1093/cercor/bhab469
18. Hu Y, Zhu M, Liu Y, Wang Z, Cheng X, Pan Y, Hu Y (2022) Musical Meter Induces Interbrain Synchronization during Interpersonal Coordination. *Eneuro*, *9*(5), ENEURO.0504-21.2022. https://doi.org/10.1523/ENEURO.0504-21.2022
19. Jia T, Sun J, McGeady C, Ji L, Li C (2024) Enhancing Brain–Computer Interface Performance by Incorporating Brain-to-Brain Coupling. Cyborg Bionic Syst 5. https://doi.org/10.34133/cbsystems.0116
20. Konvalinka I, Bauer M, Stahlhut C, Hansen LK, Roepstorff A, Frith CD (2014) Frontal alpha oscillations distinguish leaders from followers: Multivariate decoding of mutually interacting brains. NeuroImage 94:79–88. https://doi.org/10.1016/j.neuroimage.2014.03.003
21. Konvalinka I, Roepstorff A (2012) The two-brain approach: how can mutually interacting brains teach us something about social interaction? *Frontiers in Human Neuroscience*, *6*. https://doi.org/10.3389/fnhum.2012.00215
22. Lachaux JP, Rodriguez E, Martinerie J, Varela FJ (1999) Measuring phase synchrony in brain signals. Hum Brain Mapp 8(4):194–208. https://doi.org/10.1002/(sici)1097-0193(1999)8:4%3C194::aid-hbm4%3E3.0.co;2-c
23. Leahy O, Kontaris E, Gunasekara N, Hirsch J, Tachtsidis I (2025) Environmental effects on inter-brain coupling: a systematic review. *Frontiers in Human Neuroscience*, *19*. https://doi.org/10.3389/fnhum.2025.1627457
24. Li Y, Wang Y, Su C, Deng F, Pan Y (2025) Bidirectional information flow in cooperative learning reflects emergent leadership. Commun Biology 8(1):1000. https://doi.org/10.1038/s42003-025-

08445-6

25. Lindenberger U, Li S-C, Gruber W, Müller V (2009) Brains swinging in concert: Cortical phase synchronization while playing guitar. BMC Neurosci 10(1):22
26. Mu Y, Guo C, Han S (2016) Oxytocin enhances inter-brain synchrony during social coordination in male adults. Soc Cognit Affect Neurosci 11(12):1882–1893. https://doi.org/10.1093/scan/nsw106
27. Müller V, Sänger J, Lindenberger U (2013) Intra- and Inter-Brain Synchronization during Musical Improvisation on the Guitar. PLoS ONE 8(9):e73852. https://doi.org/10.1371/journal.pone.0073852
28. Müller V, Sänger J, Lindenberger U (2018) Hyperbrain network properties of guitarists playing in duet. Ann N Y Acad Sci 1423(1):198–210
29. Pan Y, Novembre G, Song B, Li X, Hu Y (2018) Interpersonal synchronization of inferior frontal cortices tracks social interactive learning of a song. NeuroImage 183:280–290. https://doi.org/10.1016/j.neuroimage.2018.08.005
30. Rai LA, Lee H, Becke E, Trenado C, Abad-Hernando S, Sperling M, Vidaurre D, Wald-Fuhrmann M, Richardson DC, Ward JA, Orgs G (2025) Delta-band audience brain synchrony tracks engagement with live and recorded dance. IScience 28(7):112922. https://doi.org/10.1016/j.isci.2025.112922
31. Rubinov M, Sporns O (2010) Complex network measures of brain connectivity: Uses and interpretations. NeuroImage 52(3):1059–1069. https://doi.org/10.1016/j.neuroimage.2009.10.003
32. Sänger J, Müller V, Lindenberger U (2012) Intra- and interbrain synchronization and network properties when playing guitar in duets. *Frontiers in Human Neuroscience*, *6*. https://doi.org/10.3389/fnhum.2012.00312
33. Sänger J, Müller V, Lindenberger U (2013) Directionality in hyperbrain networks discriminates between leaders and followers in guitar duets. *Frontiers in Human Neuroscience*, *7*. https://doi.org/10.3389/fnhum.2013.00234
34. Sawicki J (2025) *Adaptation and synchronization -- basic mechanisms in music performance*
35. Seth AK, Barrett AB, Barnett L (2015) Granger Causality Analysis in Neuroscience and Neuroimaging. J Neurosci 35(8):3293–3297. https://doi.org/10.1523/JNEUROSCI.4399-14.2015
36. Tafreshi TF, Daliri MR, Ghodousi M (2019) Functional and effective connectivity based features of EEG signals for object recognition. Cogn Neurodyn 13(6):555–566. https://doi.org/10.1007/s11571-019-09556-7
37. Tomyta K, Saito N, Ohira H (2023) The physiological basis of leader-follower roles in the dyadic alternating tapping task. *Frontiers in Psychology*, *14*. https://doi.org/10.3389/fpsyg.2023.1232016
38. Tran X-T, Vo T-N, Vu S-T, Tran T-T, Nguyen M-D, Do T, Lin C-T (2026) Inter- and intra-subject variability in EEG: A systematic survey. arXiv preprint. https://doi.org/10.48550/arXiv.2602.01019
39. Vanzella P, Balardin JB, Furucho RA, Morais Z, Janzen GAB, Sammler T, D., Sato JR (2019) fNIRS Responses in Professional Violinists While Playing Duets: Evidence for Distinct Leader and Follower Roles at the Brain Level. Front Psychol 10:164. https://doi.org/10.3389/fpsyg.2019.00164

40. Yoneta N, Watanabe H, Shimojo A, Takano K, Saito T, Yagyu K, Shiraishi H, Yokosawa K, Boasen J (2022) Magnetoencephalography Hyperscanning Evidence of Differing Cognitive Strategies Due to Social Role During Auditory Communication. *Frontiers in Neuroscience*, *16*. https://doi.org/10.3389/fnins.2022.790057
41. Zamm A, Palmer C, Bauer A-KR, Bleichner MG, Demos AP, Debener S (2021) Behavioral and Neural Dynamics of Interpersonal Synchrony Between Performing Musicians: A Wireless EEG Hyperscanning Study. Front Hum Neurosci 15. https://doi.org/10.3389/fnhum.2021.717810
42. Zhou G, Bourguignon M, Parkkonen L, Hari R (2016) Neural signatures of hand kinematics in leaders vs. followers: A dual-MEG study. NeuroImage 125:731–738. https://doi.org/10.1016/j.neuroimage.2015.11.002

Figures

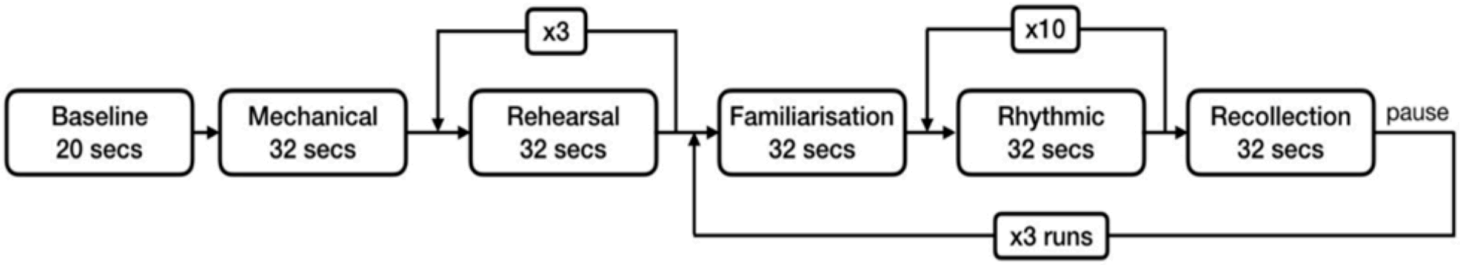


Figure 1

Sequence of recording protocol for each session.

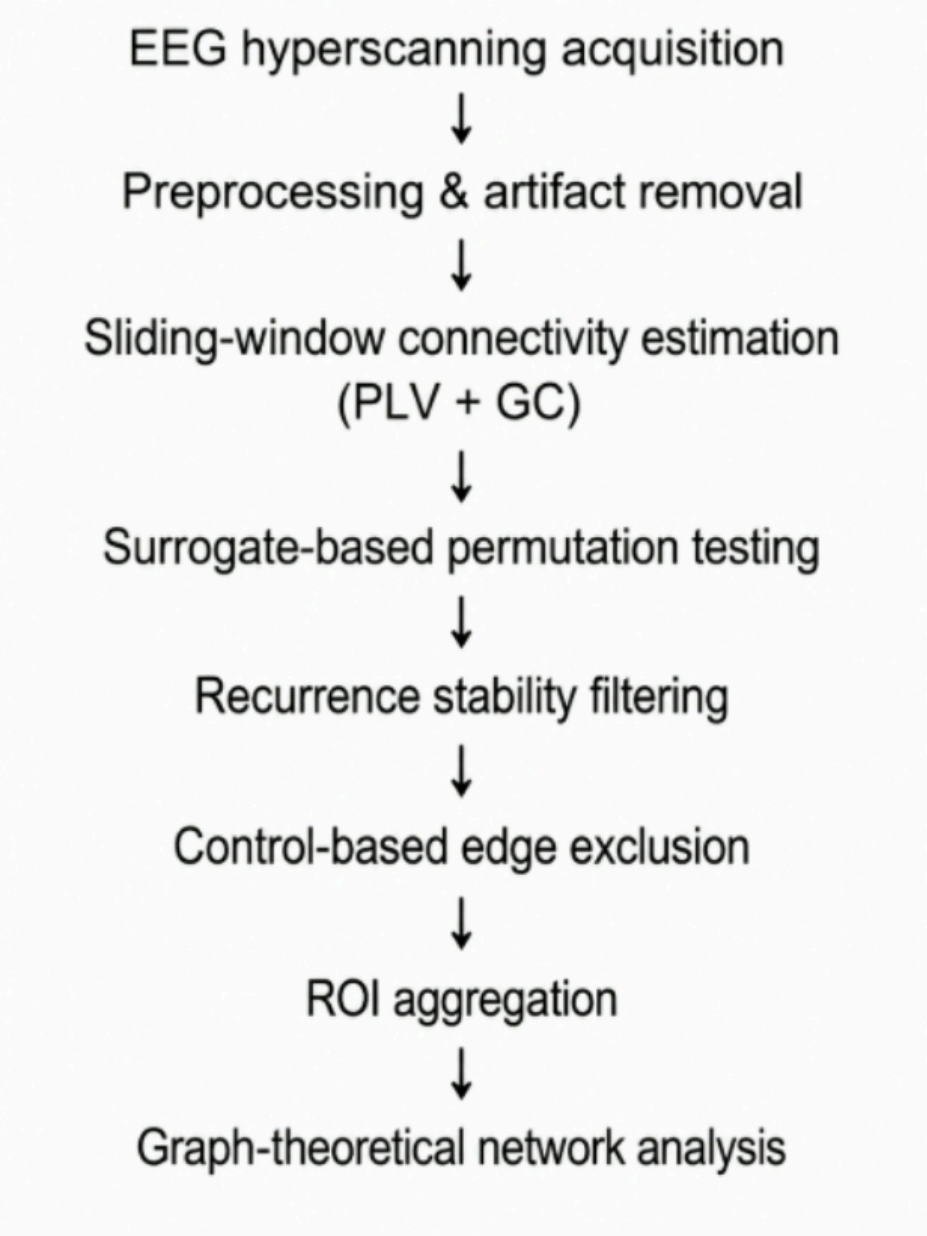


Figure 2

Overview of the proposed EEG hyperscanning connectivity framework. The pipeline includes preprocessing, sliding-window estimation of phase-locking value (PLV) and Granger causality (GC), surrogate-based permutation testing, recurrence-based stability filtering, control-based edge exclusion, ROI-level dimensionality reduction, and graph-theoretical network analysis.

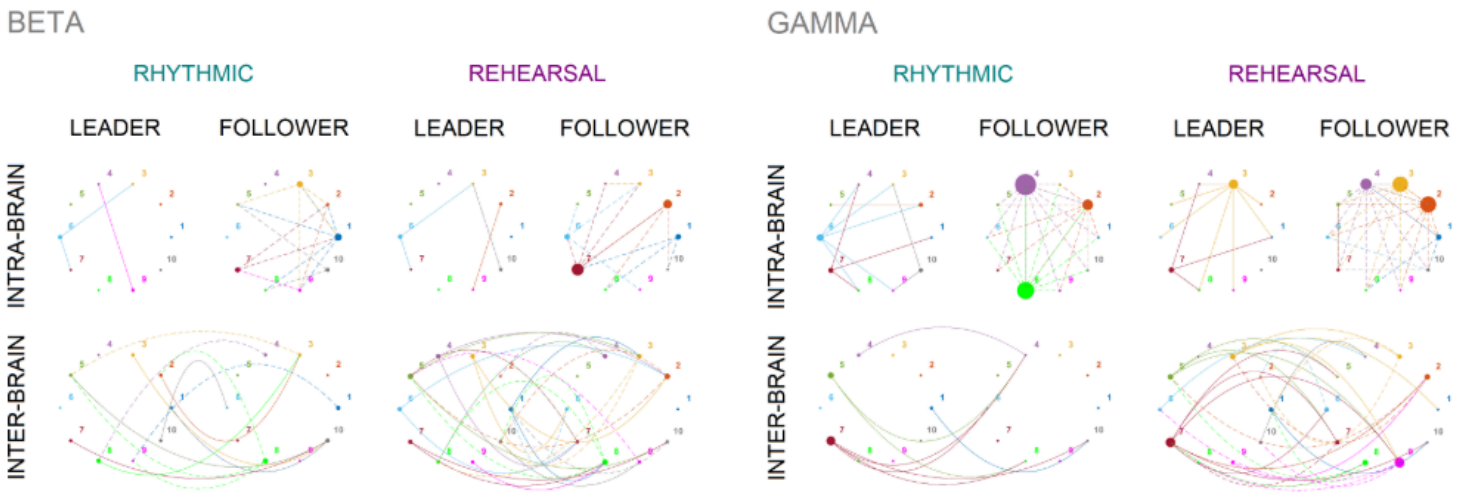


Figure 3

Control-filtered and averaged intra- and inter-brain GC connections. Colors represent predefined anatomical ROIs (also coded as numbers: mid-frontal left (1) and right (2), fronto-lateral left (3) and right (4), centro-parietal left (5) and right (6), parieto-occipital left (7) and right (8), fronto-central (9) and central parieto-occipital (10)) and corresponding connections from each ROI. For the leader, solid lines are used; for the follower, dashed lines are used. The size of the nodes reflects Node Degree.

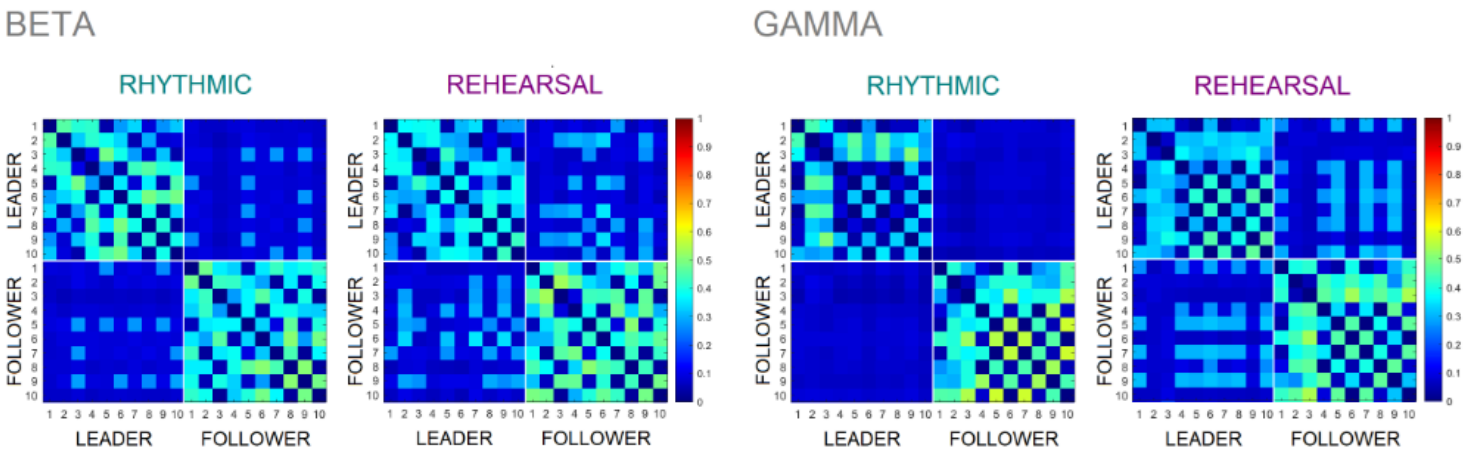


Figure 4

Control-filtered group-averaged PLV connectivity plots. The color scale (0–1) represents the mean strength of each connection across all trials and sessions, with warmer hues reflecting stronger synchrony.

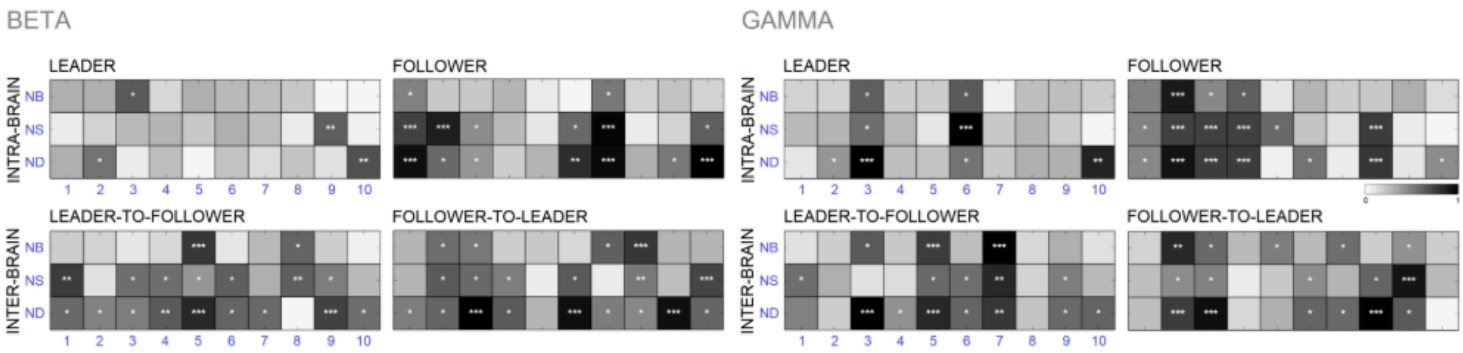


Figure 5

ROI-level heatmaps of effect sizes and corresponding p-values for significant differences between the Rhythmic and Rehearsal conditions based on GC-derived graph metrics: Node Betweenness (NB), Node Strength (NS), and Node Degree (ND). Color intensity represents the mean |Cohen's d|across the 27 LOFO iterations, with darker colors representing larger effects; the displayed scale is restricted to the range shown for visualization. Asterisks denote statistical significance (p < 0.05, ** p < 0.01, *** p < 0.005).*

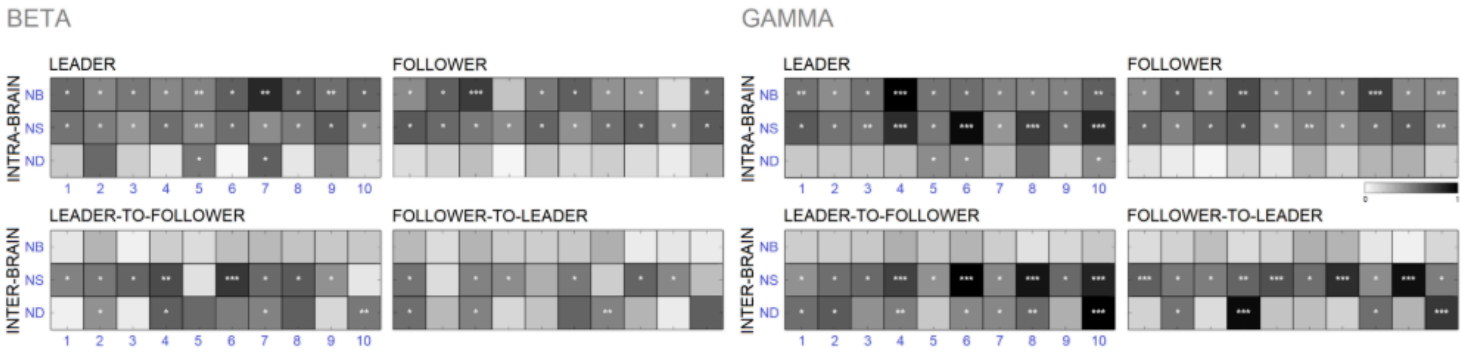


Figure 6

ROI-level heatmaps of effect sizes and corresponding p-values for significant differences between the Rhythmic and Rehearsal conditions based on PLV-derived graph metrics: Node Betweenness (NB), Node Strength (NS), and Node Degree (ND). Color intensity represents the mean |Cohen's d| across the 27 LOFO iterations, with darker colors representing larger effects; the displayed scale is restricted to the range shown for visualization. Asterisks denote statistical significance (p < 0.05, ** p < 0.01, *** p < 0.005).*

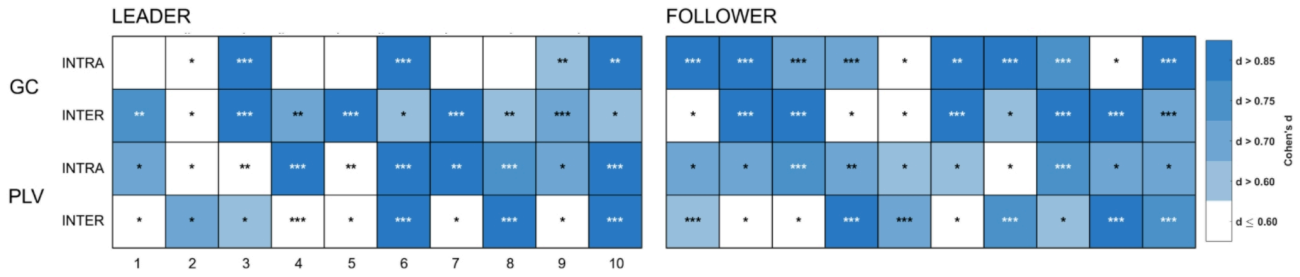


Figure 7

Heatmaps of ROI-level statistical significance and corresponding effect sizes across GC and PLV measures for the leader (left) and follower (right). White indicates mean |Cohen's d*| < 0.60, while blue shades represent mean |Cohen's* d*| ≥ 0.60. Asterisks denote significance levels (*p < 0.05, **p < 0.01, ***p < 0.005).*